Available online at www.sciencedirect.com

Manufacturing Letters

Manufacturing Letters 44 (2025) 1649–1656

53rd SME North American Manufacturing Research Conference (NAMRC 53, 2025)

Comparison of 3D-Printed Copper Surfaces for Enhanced Pool Boiling Heat Transfer

Abishek Balsamy-Kamaraj[a], Md Moynul Hasan[b], Saketh Merugu[b], Anju Gupta[b,*]

[a]*School of Engineering, Grand Valley State University, Grand Rapids, MI, 49504, USA*
[b]*Department of Mechanical, Industrial and Manufacturing Engineering, University of Toledo, Toledo, OH, 43606, USA*

* Corresponding author. Tel.: +1-419-530-8213. *E-mail address:* anju.gupta@utoledo.edu

Abstract

Efficient thermal management is increasingly crucial in various industries, including electronics, automotive, aerospace, and medical devices. Pool boiling, a highly effective two-phase heat transfer method, offers significant potential for heat dissipation. This study evaluates the performance of six distinct 3D-printed Copper Thermal Enhancement Surfaces (3D-TES) in pool boiling applications. This study investigated geometries including various surface patterns based on linear structures, wave-like formations, angular designs, and channel configurations. These surfaces were engineered to optimize three critical factors: nucleation site density, vapor escape pathways, and liquid rewetting characteristics, all of which are crucial for increasing critical heat flux (CHF). Performance evaluation was conducted using the CHF enhancement factor (ER_{CHF}) and enhancement index (EI). Among the tested geometries, the vertical wave structure demonstrated superior performance, achieving up to 260% CHF improvement with ethanol. This was attributed to the synergistic effect of increased surface area and roughness, where roughness enhances active nucleation sites while the larger area amplifies bubble generation. Additionally, wicking along the wavy walls promotes liquid replenishment, improving wetting and delaying dryout.

Peer-review under responsibility of the scientific committee of the NAMRI/SME.
Keywords: 3D-printed thermal enhancement surfaces; Fused deposition modeling, Boiling, Heat transfer, Enhancement index

1. Introduction

Two-phase heat transfer phenomena are critical in power generation [1], nuclear reactors [2], and electronics cooling [3], due to their ability to transfer large amounts of heat while maintaining low surface temperatures [4, 5]. Pool boiling, a key mode of two-phase heat transfer, has attracted significant attention for its potential to enhance thermal performance [6]. Strategies such as surface modifications [7, 8], thermally conductive fluid additives and nanofluids [9], binary mixtures [10], and nature-inspired geometries [11] have been explored to improve heat transfer efficiency.

Additively manufactured (AM) 3D-printed thermal enhancement surfaces (3D-TES) have emerged as a promising solution for enhancing pool boiling heat transfer performance. These surfaces allow for precise control over surface geometries, which is critical for influencing nucleation sites, defined as microscopic cavities with small openings that trap gas bubbles and initiate boiling at low wall superheats [12]. By increasing the number and optimizing the distribution of these nucleation sites, 3D-TES enhance vapor generation and improve heat transfer rates significantly [13, 14]. These enhanced surfaces also help control surface wettability and capillary effects, contributing to enhanced

boiling performance [13, 15]. Building upon the advancements in surface engineering, AM offers unique capabilities that extend beyond traditional manufacturing methods. Among the various AM techniques available, Material Extrusion also known as Fused Deposition Modeling (FDM), Powder bed fusion also referred to as Selective Laser

Peer-review under responsibility of the scientific committee of the NAMRI/SME.

Sintering (SLS), and Stereolithography (SLA) have gained attention for their ability to fabricate highly complex surface structures tailored for heat transfer applications [16-18]. The layer-by-layer deposition process characteristic of FDM enables the creation of intricate surface features that are essential for optimizing heat transfer in pool boiling applications.

The ability of FDM to fabricate internal channels and structures, combined with its compatibility with metal-filled filaments such as copper composites, further enhances the thermal conductivity of the surfaces produced. This makes FDM particularly useful for designing heat exchangers, heat sinks, and other thermal management components that require both structural complexity and high thermal resistance [19-21]. Moreover, while techniques such as SLS and SLA provide smoother surface finishes and higher resolution, FDM-printed surfaces have the advantage of inherent surface roughness. This roughness, rather than being a drawback, can improve boiling heat transfer performance by promoting capillary wicking and enhancing wettability. As a result, versatility of FDM in material choice (such as copper) and surface design offers a distinct advantage for improving pool boiling efficiency, making it an attractive option for further exploration in industrial heat transfer applications. Compared to previous studies, particularly the review by Kumar and Negi [14] on additive manufacturing-based surface modifications for pool boiling, our study introduces novel geometries and working fluid combinations to further enhance critical heat flux (CHF). While earlier research explored various surface geometries, our investigation of six distinct 3D-TES (3D-printed Thermal Enhancement Surfaces) demonstrates significant CHF improvements, especially with ethanol. Additionally, our study extends the analysis to water-ethanol mixtures, offering new insights into fluid-surface interactions, highlighting the potential of structured surfaces for advanced cooling applications.

In this study, we investigated the pool boiling performance of six distinct copper 3D-TES -, arced, chevron, horizontal wave, straight, square duct, and vertical wave with DI water, ethanol, and water-ethanol mixtures as working fluids. The fin geometries were selected to enhance boiling heat transfer by promoting improved nucleation site density, optimized vapor escape, and efficient liquid rewetting, which are key to increasing CHF. To evaluate the performance of these surfaces, we calculated and reported the ER_{CHF} and EI for all surfaces with four working fluids. By tailoring the surface geometry, each fin type offers potential improvements in pool boiling performance across a range of fluid compositions. This study aims to provide valuable insights into how surface design and fluid properties interact to influence boiling efficiency, contributing to the ongoing development of advanced thermal management solutions for applications such as electronics cooling and energy storage systems. applications such as electronics cooling and energy storage.

Nomenclature

CHF	critical heat flux (kW/m^2)
HTC	heat transfer coefficient ($kW/m^2.°C$)
q"	heat flux (kW/m^2)
k_{Cu}	thermal conductivity of copper ($W/m°.C$)
T_{wall}	surface temperature of the copper substrate (°C)
T_{sat}	saturation temperature of the working fluid (°C)
ΔT	wall superheat (°C)
WS	wall superheat (°C)
3D-TES	3D-printed Thermal Enhancement Surfaces
ER_{CHF}	CHF enhancement factor
EI	enhancement index
FDM	fused deposition modeling

2. Materials and methods

2.1. Preparation of 3D-Thermal enhancement surfaces

Six 3D-TES designs were inspired from commercially available heat sinks, prioritizing heat transfer performance [22, 23]. To ensure consistency, all six samples were printed in a single batch. As shown in Fig. 1, all six 3D-TES were arranged on the build plate in an orientation selected to minimize support structures and optimize wall thickness uniformity, aligning with standard copper filament printing practices. This approach ensured uniformity across samples and reduced potential variability in the results.

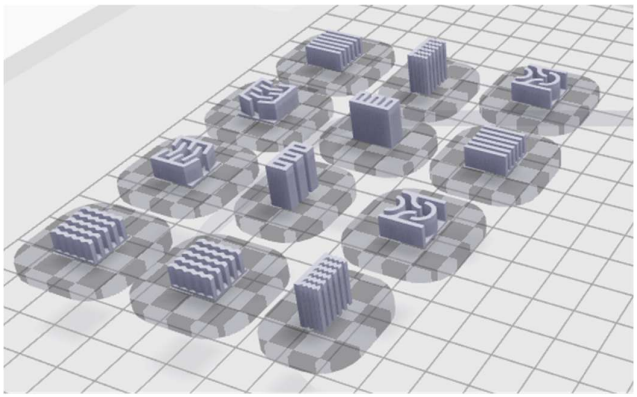

Fig. 1. 3D-TES orientation on the build plate.

Each structured surface was designed to fit within a 10 mm × 10 mm × 5 mm volume, a size chosen to align with the experimental setup requirements. However, slightly larger structures, such as those scaled 2x or 5x, have a minimal effect on surface properties. In contrast, an order-of-magnitude increase in size may result in increased surface roughness due to more pronounced layer lines [24]. The structured surface models were sliced using the proprietary Markforged software, Eiger. To account for shrinkage during sintering, the surfaces were printed with an approximate 20% scale-up. The dimensions of the features were constrained by the minimum feature size of the Metal X fused deposition modeling printer, with vertical structural boundaries (referred to as walls)

forming enhancement features such as fins or lattice edges. These walls had a minimum thickness of 1.0 mm and a maximum of 2.5 mm. The 3D printing parameters included adaptive layer heights ranging between 50 and 175 µm, while nozzle temperature and other critical settings remained proprietary to the manufacturer. These parameters were selected to ensure consistent quality and structural integrity of the printed parts. The surfaces were oriented for printing without support material or rafts at the base. After printing, the green parts underwent washing in the Markforged Wash-1 system, which employs heat and a fluorinated solvent (similar to Opteon SF79) to remove the polymer binder. The parts were then sintered into their final form using the Markforged Sinter-1 furnace. The sintering process involved two stages: solvent debinding, where green parts were immersed in the fluorinated solvent for approximately 12 hours, followed by high-temperature sintering under an argon atmosphere. The sintering cycle included a controlled ramp and hold profile, heating to 1040–1080°C over 24–26 hours to achieve full densification and near-wrought copper density. No additional post-processing was conducted. However, the printed copper structured surfaces exhibited warping, which could hinder heat transfer between the heat source and fluid medium. Due to copper's inherently low hardness, the unsintered parts were extremely fragile. The decision to print without rafts aimed to avoid warping during raft removal post-sintering; however, this increased the risk of pre-sintering warping. Warped bottom plates were particularly problematic, as non-flat bases would reduce the contact surface area between the structured surface and the heat source. Reduced contact area diminishes conductive heat transfer, lowering the rate at which heat is transferred from the source to the fluid medium. To mitigate this, the sintered structured surfaces were soldered to plain copper plates prior to conducting pool boiling experiments.

2.2. Pool boiling setup

The pool boiling experimental setup shown in Fig. 2 consists of a test section, a working fluid reservoir, and a heater block. The copper substrate is enclosed in a ceramic holder with low thermal conductivity to minimize heat loss from the sides, ensuring that the heat transfer remains primarily unidirectional from the heater block to the test surface. A working fluid reservoir measuring 14 mm x 14 mm x 38 mm is sealed using rubber gaskets to prevent leakage, and a Kapton® tape with a thermal conductivity of 0.2 W/m-K is used to insulate the exposed areas outside the boiling surface. Three K-type thermocouples are placed in pre-drilled holes on the copper substrate at varying distances from the boiling surface, allowing for real-time temperature measurements. The data acquisition is managed through a National Instruments cDAQ-9172 system with a 9213-thermocouple input module. During the experiments, the system records the temperatures and computes the necessary parameters, including heat flux and surface temperature. The heat flux (q'') is calculated using the following equation:

$$q'' = -k_{Cu}\frac{dT}{dx} \quad (1)$$

Where k_{Cu} is the thermal conductivity of copper, and $\frac{dT}{dx}$ is the temperature gradient. The temperature gradient $\frac{dT}{dx}$ is computed using a three-point backward Taylor series approximation:

$$\frac{dT}{dx} = \frac{3T_1 - 4T_2 + T_3}{2\Delta x} \quad (2)$$

Where T_1, T_2, and T_3 are the temperatures measured by the thermocouples at different points on the substrate, and Δx is the distance between the thermocouples. The wall temperature (T_{wall}) is calculated as:

$$T_{wall} = T_1 - q''\frac{x_1}{k_{Cu}} \quad (3)$$

Where x_1 is the distance between the boiling surface and the first thermocouple. Finally, the heat transfer coefficient (HTC) is computed as:

$$HTC = \frac{q''}{T_{wall} - T_{sat}} \quad (4)$$

Where T_{sat} is the saturation temperature of the working fluid. This setup was validated in our previous study [25], demonstrating the accuracy of temperature measurements and heat flux calculations, and showing good agreement with relevant literature data [26-29].

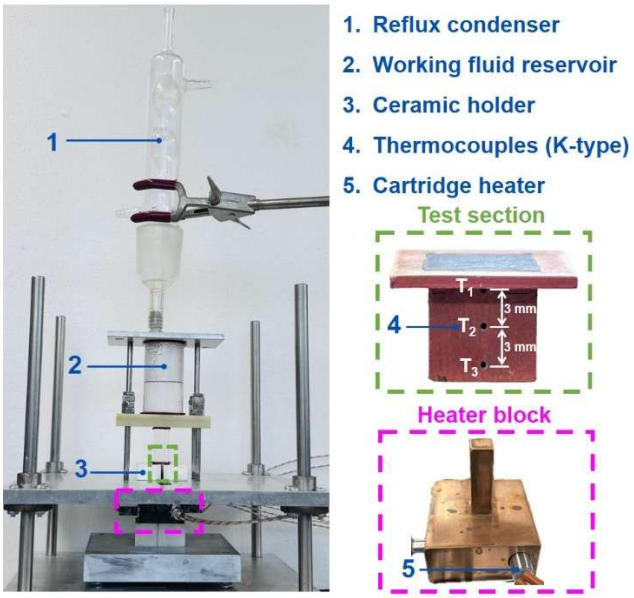

Fig. 2. The experimental pool boiling setup.

3. Results and discussion

3.1. Thermal performance evaluation of 3D-TES

The thermal performance of the 3D-TES for cooling applications, such as electronics cooling, automotive heat management systems, and thermal control in aerospace and medical devices, requires more stringent standards compared to heat exchangers. The heat transfer enhancement achieved by 3D-TES through pool boiling is evaluated by comparing the

performance of 3D-TES with a plain copper surface with no surface modifications, which serves as a standard benchmark in pool boiling studies [30, 31]. To ensure a fair and accurate comparison, we conducted a comparative analysis of the CHF of 3D-TES structures against that of plain copper for each coolant. For example, the CHF of 3D-TES with water was compared to the CHF of plain copper with water. The CHF and HTC, calculated using Eq 1 and Eq 4 for different surfaces, are further used to calculate the CHF and HTC enhancement factors, as formulated by Shukla and Kandlikar [32]. The ER_{CHF} is the ratio of the CHF of the enhanced surface to that of the plain surface for the same working fluid, as given by:

$$ER_{CHF} = \frac{q"_{CHF,E}}{q"_{CHF,Plain}} \quad (5)$$

where $q"_{CHF,E}$ is the CHF of the enhanced surface and $q"_{CHF,Plain}$ is the CHF of the plain surface. Similarly, the HTC enhancement factor (ER_{HTC}) for the same working fluid is given by:

$$ER_{HTC} = \frac{h_{HTC,E}}{h_{HTC,Plain}} \quad (6)$$

where $q"_{HTC,E}$ and $q"_{HTC,Plain}$ are the heat transfer coefficients at CHF for the enhanced and plain surfaces, respectively. To further evaluate performance, the enhancement index (EI) is employed for the same working fluid, accounting for the wall superheat at CHF conditions on both surfaces:

$$EI = \frac{\Delta T_{CHF,E}}{\Delta T_{CHF,Plain}} = \frac{q"_{CHF,E}}{q"_{CHF,Plain}} \times \frac{h_{HTC,Plain}}{h_{HTC,E}} = \frac{ER_{CHF}}{ER_{HTC}} \quad (7)$$

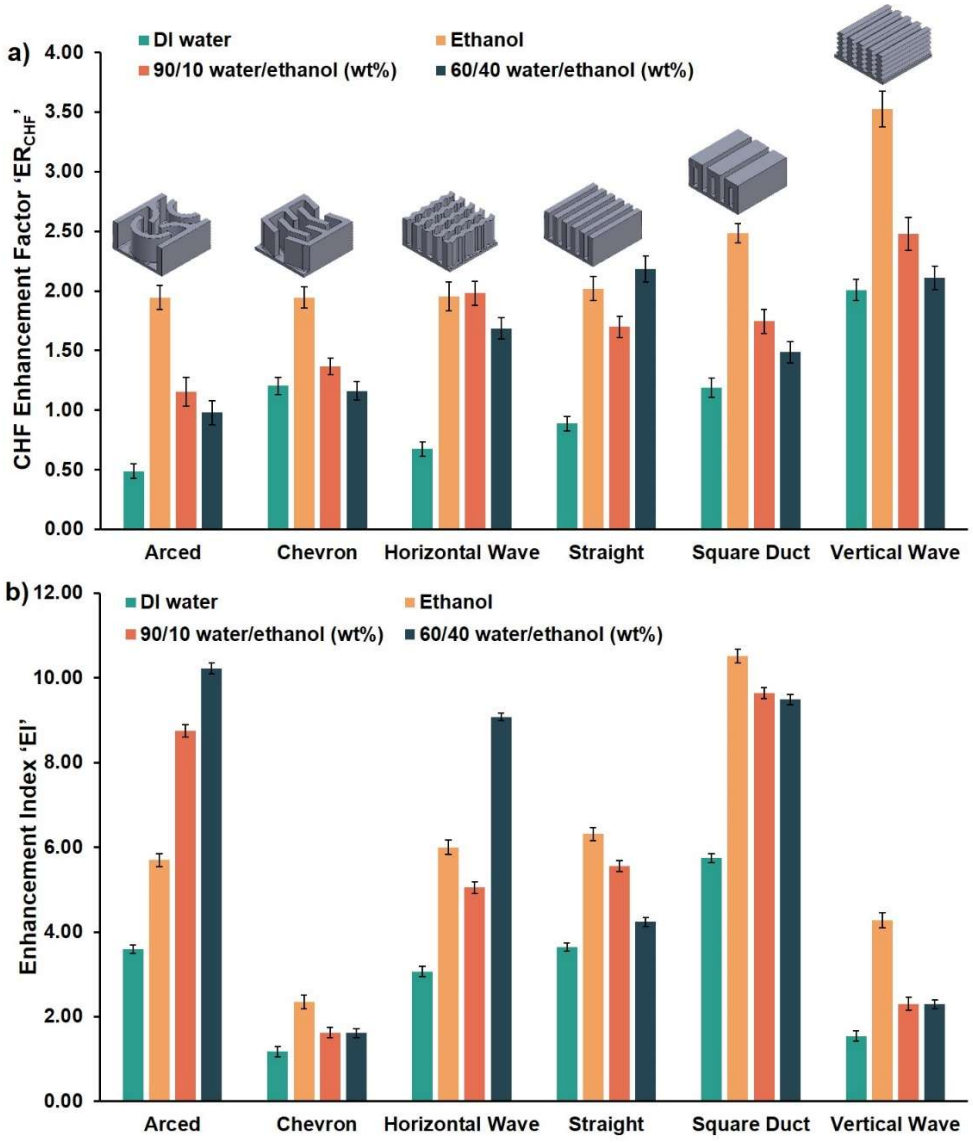

Fig. 3. 3D-TES pool boiling performance enhancement metrics, a) ER_{CHF}, b) EI with DI water, ethanol, 90/10, and 60/40 water /ethanol (wt%) as working fluids.

These enhancement factors were used to assess the performance of the six 3D-TES. To ensure accuracy and consistency, the pool boiling experiments were triplicated for each of the six 3D-TES designs. The calculated enhancement metrics for the six 3D-TES, along with their geometries, are shown in Fig. 3. The ER_{CHF} and EI were calculated for four working fluids: DI water, ethanol, 90/10 water/ethanol (wt%), and 60/40 water/ethanol (wt%). The ER_{CHF} is considered acceptable for cooling applications only when it is greater than 1. A higher CHF enhancement factor (ER_{CHF}) indicates a greater ability of the 3D-TES to remove heat from the surface. For DI water as the working fluid, the vertical wave surface had the highest calculated ER_{CHF} of 2, followed by the chevron surface with an ER_{CHF} of 1.2. The 3D-TES demonstrated significantly better ER_{CHF} with ethanol and water/ethanol binary mixtures. Although changes in ER_{CHF} partly arise from surface geometry, variations in fluid properties and interfacial phenomena also play a critical role. For instance, the lower surface tension of ethanol reduces bubble departure diameter, while in binary mixtures, surface tension gradients [33] and thermal diffusion [34] enhance fluid replenishment and alter nucleation dynamics [11]. Consequently, the highest calculated ER_{CHF} values were 3.53 for the vertical wave surface with ethanol and 2.48 for the vertical wave surface with the 90/10 water/ethanol binary mixture. These high ER_{CHF} demonstrate the potential of the vertical wave surface for superior cooling applications. While the vertical wave surface had the highest ER_{CHF} across all working fluids, other surfaces also showed improved pool boiling performance compared to plain copper. A high ER_{CHF} demonstrates the enhanced performance of 3D-TES; however, it must be accompanied by a low EI to ensure stable and energy-efficient cooling. The lower the EI, the greater the ability of the surface to maintain a low surface temperature. This balance between high heat flux and low surface temperature is essential for maintaining the longevity and reliability of cooling systems, especially in applications where continuous heat removal is critical. The calculated EI for the six 3D-TES is shown in Fig. 3b. The lowest calculated EI values of 1.18 and 1.54 were recorded for the chevron and vertical wave surfaces, respectively, when using DI water. In the case of ethanol and binary mixtures, the chevron surface had the lowest EI, followed by the vertical wave surface. These results highlight the importance of surface geometry and its influence on the ability to manage heat efficiently across different fluid types. The other 3D-TES performed poorly in terms of their ability to maintain low surface temperatures. The overall pool boiling performance depends on the combined effect of ER_{CHF} and EI. A surface with an ER_{CHF} greater than 3 and an EI less than 0.5 is considered highly desirable, representing ultra-high-performance enhancement. The vertical wave structure demonstrated a very high ER_{CHF}, and a relatively low EI compared to most other 3D-TES, while the chevron structure exhibited the lowest EI among all tested surfaces. However, the vertical wave structure stands out as the most effective design due to its combination of high ER_{CHF} and low EI.

3.2. Enhanced thermal performance of Vertical wave 3D-TES for different working fluids

Since heat removal in phase-change processes is influenced by fluid surface tension, it is critical for enhanced surfaces to be designed to effectively utilize working fluids across a broad range of surface tensions. To investigate how varying surface tension affects phase-change behavior while maintaining water as the primary solvent, we selected two extreme ethanol concentrations: 90/10 wt% and 60/40 wt%. The 90/10 mixture reduces the surface tension compared to pure water, whereas the 60/40 mixture lowers it further due to the higher ethanol content [35]. By choosing these boundary compositions, we capture the influence of ethanol addition on boiling characteristics and CHF over a practical range, thus providing a comprehensive evaluation of phase-change performance. In our study, we observed significant differences in heat transfer characteristics and boiling behavior between water and binary mixtures. Ethanol, with a surface tension of 22.1 mN/m compared to 72.8 mN/m for water, results in a higher frequency of bubbles that carry away heat, enhancing CHF even at low heat fluxes. This behavior is amplified in mixtures due to surface tension gradients between water and ethanol that drive fluid flow from ethanol-rich regions with lower surface tension to water-rich regions with higher surface tension, enhancing liquid rewetting and delaying dryout [11]. This explains the high ER_{CHF} for ethanol and binary mixtures for all 3D-TES, as shown in Fig. 3a. For the vertical wave, all four working fluids demonstrated high ER_{CHF} and low EI. Fig. 4 shows the heat flux vs. WS pool boiling curves with different working fluids for the vertical wave 3D-TES. The data was collected by gradually increasing the heat flux until CHF was reached.

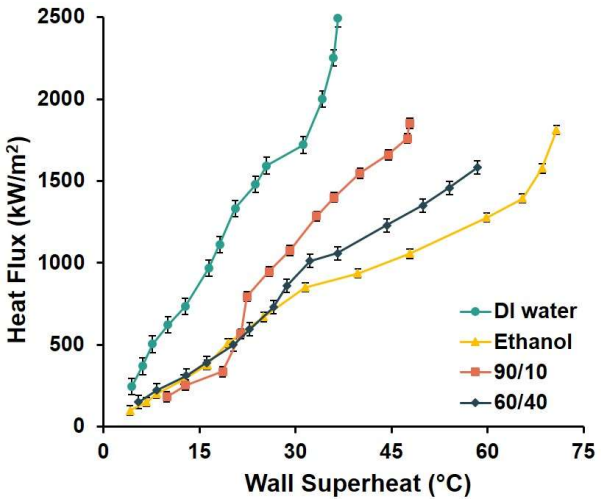

Fig. 4. Pool boiling curves of vertical wave 3D-TES for water, ethanol, 90/10, and 60/40 water/ethanol (wt%) as working fluids.

At CHF, a vapor film forms on the surface, preventing any further heat transfer. For DI water, the vertical wave surface reached CHF at approximately 2500 kW/m² with a WS of about 36 °C, compared to 1250 kW/m² at 24 °C for plain Cu, which

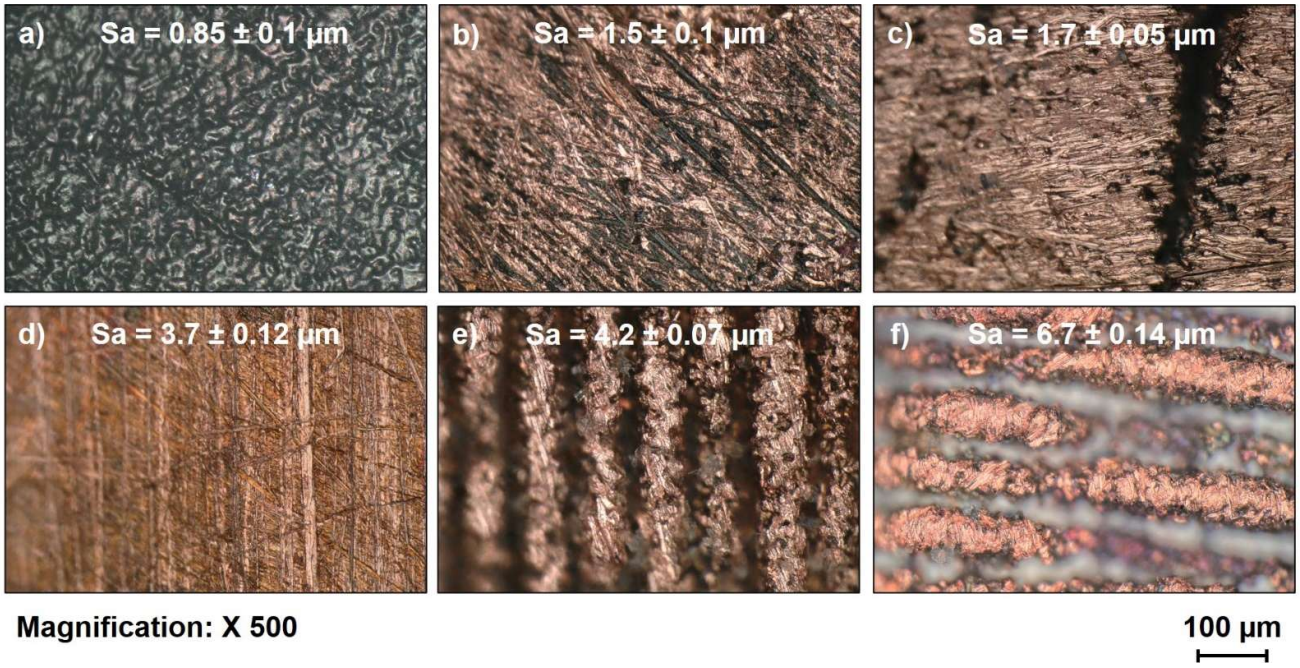

Fig. 5. Electron microscopy images of 3D-TES, a) arced, b) chevron, c) horizontal wave, d) straight, e) square duct, and f) vertical wave.

represents a 100% increase in CHF but at a 50% higher surface temperature. For ethanol, the vertical wave reached CHF at 1800 kW/m² with a WS of 70 °C, while the CHF of plain Cu with ethanol was 500 kW/m² at 17 °C. This represents around a 260% increase in CHF for the vertical wave with ethanol, although at the cost of higher WS. This increase in heat transfer rates may be attributed to the increased surface area of the vertical wave 3D-TES structures. Additionally, the increase in the number of active nucleation sites due to enhanced surface roughness increases bubble frequency and density, thereby improving heat transfer performance [36]. Electron microscopy images in Fig. 5 confirm that the vertical wave 3D-TES exhibits the highest surface roughness measurements, with an arithmetical mean height (Sa) of 6.7 ± 0.14 µm, surpassing all other 3D-TES designs. Furthermore, the maximum height (Sz) of the vertical wave structure is 21.4 ± 0.3 µm, the highest among the designs, while the arced structure has the lowest Sz value of 11.1 ± 0.17 µm. Additionally, these wave-like structures create a heat conduction path along the height of the structures. Although the increase in wall superheat cannot be overlooked compared to plain Cu, it is crucial to note that the vertical wave 3D-TES yielded high CHF with all working fluids. This improvement outweighs the need for low WS in many applications. Fig. 6 shows other contributing factors and mechanisms that we propose that led to the enhanced performance of the vertical wave 3D-TES. Fig. 6a shows high-speed camera images of bubble nucleation from the rough walls of the 3D-printed structures. The rough and porous walls act as active nucleation sites from which new bubbles emerge, leading to an increase in bubble frequency and enhanced heat removal. The wicking-assisted bubble dynamics are shown in Fig. 6b, where the nucleated bubbles begin to grow, expand in size while remaining attached to the surface, and, after reaching a critical size, begin to depart. The porous surface with microscale roughness assists in bubble growth, enhances vapor

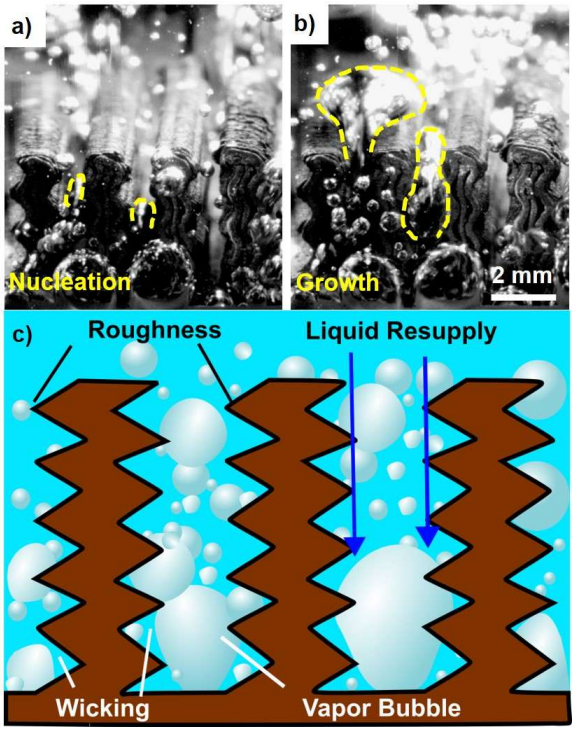

Fig. 6. Mechanisms behind vapor bubble dynamics of vertical wave 3D-TES demonstrated using high speed camera images of vapor bubble a) nucleation, b) growth, and c) schematic of mechanisms influencing bubble dynamics for all working fluids.

rise, and improves bubble dynamics. Fig. 6c demonstrates the proposed synergistic effect of microscale roughness and macroscale interpillar spacing on bubble dynamics for the 3D-printed vertical wave thermal enhancement surface. The wavy grooves on the walls aid in wetting the walls through continuous wicking, preventing dryout and keeping the nucleation sites active for further bubble growth. The interpillar spacing and microscale roughness facilitate liquid resupply along the pillar walls due to capillary effects. The departing bubbles create a low-pressure zone, which pulls in cooler water and pushes the hot water upward, creating a cycle of bubble growth and departure along the walls of the 3D-printed surface, resulting in enhanced CHF and lower wall superheat. All these mechanisms combined contributed to the improved thermal performance of the 3D-printed vertical wave thermal enhancement surface.

4. Conclusions

This study demonstrated the significant potential of 3D-printed thermal enhancement surfaces to improve pool boiling performance using DI water, ethanol, and water-ethanol mixtures as working fluids. Among the six surface designs investigated, the vertical wave structure exhibited the highest CHF enhancement factor across almost all fluids, with the greatest improvement recorded for ethanol and binary mixtures. The vertical wave surface achieved an ER_{CHF} of 3.53 with ethanol, demonstrating around a 260% increase in CHF compared to a plain copper surface, while maintaining a relatively low enhancement index, indicating efficient cooling. This exceptional performance is primarily attributed to the enhanced wetting effects along the walls due to the increased surface roughness of the vertical wave structure. The roughness-induced wetting promotes better liquid distribution and optimizes vapor escape pathways, significantly improving boiling heat transfer. The chevron surface also performed well, particularly for DI water, with a notable ER_{CHF} and low EI, showcasing its effectiveness in maintaining low surface temperatures. These results confirm that surface geometry and roughness play critical roles in improving boiling heat transfer, with optimized nucleation site density, vapor escape pathways, and liquid rewetting contributing to these enhancements. The study highlights the advantages of Fused Deposition Modeling for creating 3D-TES, especially for applications requiring both high heat flux removal and structural complexity. The ability to control surface roughness through 3D printing techniques proves to be a key factor in enhancing boiling performance. Future work should focus on further optimizing these designs for industrial applications, particularly in electronics cooling and energy storage, where enhanced thermal management is essential. Special attention should be given to leveraging and fine-tuning surface roughness to maximize wetting effects and, consequently, boiling heat transfer performance.

Credit authorship contribution statement

A.K.- Funding acquisition, Conceptualization, Project administration, Supervision, M.M.H. and S.M.- Investigation, Visualization, Methodology, Data curation, Formal analysis, Writing – original draft, A.G. Conceptualization, Project administration, Supervision, Writing- Review, Revision, and Editing.

Declaration of competing interest

The authors declare that they have no known competing financial interests or personal relationships that could have appeared to influence the work reported in this paper.

Acknowledgments

Dr. Abishek Kamaraj acknowledges the financial support provided by the US Department of Education Grant P116Z220071. Mr. Samuel Joel Menzie and aMDI, Grand Rapids are acknowledged for their help with getting the copper parts printed.

References

[1] Subhani, S., et al. Generation of Controlled Single Bubbles for Phenomenological Study of Nucleate Boiling Using a Dual-Lens Laser Spot Heating Approach. in Heat Transfer Summer Conference. 2024. American Society of Mechanical Engineers.

[2] Mokos, A., et al., Surface controlled mechanism of water boiling for nuclear reactor fuel assembly. International Journal of Heat and Mass Transfer, 2024. **230**: p. 125747.

[3] Kim, J.S., et al., Enhanced nucleate pool boiling heat transfer on CNTs-Cu nanoparticles-coated surfaces: Effects of sintering temperature and CNTs composition on pool boiling behavior. Applied Thermal Engineering, 2024. **239**: p. 122159.

[4] Hoang, C.H., et al., A review of recent developments in pumped two-phase cooling technologies for electronic devices. IEEE Transactions on Components, Packaging and Manufacturing Technology, 2021. **11**(10): p. 1565-1582.

[5] Cho, H.J., et al., Nanoengineered materials for liquid–vapour phase-change heat transfer. Nature Reviews Materials, 2016. **2**(2): p. 1-17.

[6] Katarkar, A., B. Majumder, and S. Bhaumik. Review on passive heat enhancement techniques in pool boiling heat transfer. in IOP Conference Series: Materials Science and Engineering. 2020. IOP Publishing.

[7] Qin, S., et al., Review of enhancing boiling and condensation heat transfer: Surface modification. Renewable and Sustainable Energy Reviews, 2024. **189**: p. 113882.

[8] Liang, G. and I. Mudawar, Review of pool boiling enhancement by surface modification. International Journal of Heat and Mass Transfer, 2019. **128**: p. 892-933.

[9] Liang, G. and I. Mudawar, Review of pool boiling enhancement with additives and nanofluids. International Journal of Heat and Mass Transfer, 2018. **124**: p. 423-453.

[10] Xu, J., et al., A review of boiling heat transfer characteristics in binary mixtures. International Journal of Heat and Mass Transfer, 2021. **164**: p. 120570.

[11] Rozati, S.A., M.B. Khriwish, and A. Gupta, Speleothem-Inspired Copper/Nickel Interfaces for Enhanced Liquid–Vapor Transport by Marangoni and Soret Effects. Langmuir, 2024. **40**(20): p. 10745-10758.

[12] Zohuri, B., Functionality, advancements and industrial applications of heat pipes. 2020: Academic Press.

[13] Sun, Y., et al., A review on fabrication and pool boiling enhancement of three-dimensional complex structures. Renewable and Sustainable Energy Reviews, 2022. **162**: p. 112437.

[14] Kumar, J. and S. Negi, Effect of additive manufacturing-based surface modification on pool boiling heat transfer: a review. Progress in Additive Manufacturing, 2024: p. 1-25.

[15] McDonough, J., A perspective on the current and future roles of additive manufacturing in process engineering, with an emphasis on heat transfer. Thermal Science and Engineering Progress, 2020. **19**: p. 100594.

[16] Anwajler, B., Potential of 3D Printing for Heat Exchanger Heat Transfer

Optimization—Sustainability Perspective. Inventions, 2024. **9**(3): p. 60.
[17] Zhang, Z. and X. Yuan, Applications and future of automated and additive manufacturing for power electronics components and converters. IEEE Journal of Emerging and Selected Topics in Power Electronics, 2021. **10**(4): p. 4509-4525.
[18] Jambhulkar, S., et al., Nanoparticle Assembly: From Self-Organization to Controlled Micropatterning for Enhanced Functionalities. Small, 2024. **20**(6): p. 2306394.
[19] Wickramasinghe, S., T. Do, and P. Tran, FDM-based 3D printing of polymer and associated composite: A review on mechanical properties, defects and treatments. Polymers, 2020. **12**(7): p. 1529.
[20] Choong, Y.H., M. Krishnan, and M. Gupta, Recent Advances in the 3D Printing of Pure Copper Functional Structures for Thermal Management Devices. Technologies, 2023. **11**(5): p. 141.
[21] Roudný, P. and T. Syrový, Thermal conductive composites for FDM 3D printing: A review, opportunities and obstacles, future directions. Journal of Manufacturing Processes, 2022. **83**: p. 667-677.
[22] Al-Neama, A.F., et al., An experimental and numerical investigation of chevron fin structures in serpentine minichannel heat sinks. International Journal of Heat and Mass Transfer, 2018. **120**: p. 1213-1228.
[23] Khattak, Z. and H.M. Ali, Air cooled heat sink geometries subjected to forced flow: A critical review. International Journal of Heat and Mass Transfer, 2019. **130**: p. 141-161.
[24] Hashmi, A.W., H.S. Mali, and A. Meena, The surface quality improvement methods for FDM printed parts: a review. Fused deposition modeling based 3D printing, 2021: p. 167-194.
[25] Rozati, S.A., et al., Magnetically aligned metal-organic deposition (MOD) ink based nickel/copper heater surfaces for enhanced boiling heat transfer. Applied Thermal Engineering, 2022. **211**: p. 118473.
[26] Rohsenow, W.M., A method of correlating heat-transfer data for surface boiling of liquids. Transactions of the American Society of Mechanical Engineers, 1952. **74**(6): p. 969-975.
[27] Lienhard, J. and V. Dhir, Hydrodynamic prediction of peak pool-boiling heat fluxes from finite bodies. 1973.
[28] Zuber, N., Hydrodynamic Aspects of Boiling Heat Transfer. 1959.
[29] Kandlikar, S.G., A theoretical model to predict pool boiling CHF incorporating effects of contact angle and orientation. J. Heat transfer, 2001. **123**(6): p. 1071-1079.
[30] Rozati, S.A. and A. Gupta, Enhanced Phase Change Heat Transfer with Fused Deposition Modeling (FDM) Printed Pit and Pillar (Pi2) Arrays. Experimental Thermal and Fluid Science, 2025. **161**: p. 111337.
[31] Rishi, A.M., S.G. Kandlikar, and A. Gupta, Improved wettability of graphene nanoplatelets (GNP)/copper porous coatings for dramatic improvements in pool boiling heat transfer. International Journal of Heat and Mass Transfer, 2019. **132**: p. 462-472.
[32] Shukla, M.Y. and S.G. Kandlikar, Enhancement Evaluation Criteria for Pool Boiling Enhancement Structures in Electronics Cooling: CHF Enhancement Ratio (ER-CHF) and Enhancement Index (EI). Journal of Enhanced Heat Transfer, 2024. **31**.
[33] Scriven, L. and C. Sternling, The marangoni effects. Nature, 1960. **187**(4733): p. 186-188.
[34] Köhler, W., et al., The measurement of Soret and thermodiffusion coefficients in binary and ternary liquid mixtures. International Journal of Thermophysics, 2023. **44**(9): p. 140.
[35] Khattab, I.S., et al., Density, viscosity, and surface tension of water+ ethanol mixtures from 293 to 323K. Korean Journal of Chemical Engineering, 2012. **29**: p. 812-817.
[36] Kim, J., et al., Effect of surface roughness on pool boiling heat transfer at a heated surface having moderate wettability. International Journal of Heat and Mass Transfer, 2016. **101**: p. 992-1002.